

# Amazonian landscapes and the bias in field studies of forest structure and biomass

David C. Marvin<sup>1</sup>, Gregory P. Asner, David E. Knapp, Christopher B. Anderson, Roberta E. Martin, Felipe Sinca, and Raul Tupayachi

Department of Global Ecology, Carnegie Institution for Science, Stanford, CA 94305

Edited by William J. Bond, University of Cape Town, Cape Town, South Africa, and approved October 14, 2014 (received for review July 14, 2014)

**Tropical forests convert more atmospheric carbon into biomass each year than any terrestrial ecosystem on Earth, underscoring the importance of accurate tropical forest structure and biomass maps for the understanding and management of the global carbon cycle.** Ecologists have long used field inventory plots as the main tool for understanding forest structure and biomass at landscape-to-regional scales, under the implicit assumption that these plots accurately represent their surrounding landscape. However, no study has used continuous, high-spatial-resolution data to test whether field plots meet this assumption in tropical forests. Using airborne LiDAR (light detection and ranging) acquired over three regions in Peru, we assessed how representative a typical set of field plots are relative to their surrounding host landscapes. We uncovered substantial mean biases (9–98%) in forest canopy structure (height, gaps, and layers) and aboveground biomass in both lowland Amazonian and montane Andean landscapes. Moreover, simulations reveal that an impractical number of 1-ha field plots (from 10 to more than 100 per landscape) are needed to develop accurate estimates of aboveground biomass at landscape scales. These biases should temper the use of plots for extrapolations of forest dynamics to larger scales, and they demonstrate the need for a fundamental shift to high-resolution active remote sensing techniques as a primary sampling tool in tropical forest biomass studies. The potential decrease in the bias and uncertainty of remotely sensed estimates of forest structure and biomass is a vital step toward successful tropical forest conservation and climate-change mitigation policy.

canopy structure | field inventory plots | forest carbon | Peru tropical forest | LiDAR

**U**nderstanding spatial and temporal variation in forest structure and biomass is central to the prediction of tropical forest dynamics. Forest structure is an important determinant of light use, turnover, and net primary productivity (1–3). As a result, these functional processes, which operate at leaf-to-landscape scales, drive the conversion of more atmospheric carbon each year into tropical forest biomass than any other terrestrial ecosystem on Earth (4). Maps of tropical forest aboveground biomass (AGB) are thus considered vital for forest conservation and climate change mitigation policy (5) and for understanding the role that tropical forests play in the global carbon cycle (6). However, spatially explicit maps of AGB in Amazonian forests have rarely agreed more than is expected by chance (7). Even the most recent pan-tropical AGB maps using satellite remote sensing and similar methodologies have substantial disagreement between one another (8) as well as with respect to available field-plot network estimates (9). Serious disagreement exists over our understanding of landscape and regional carbon dynamics (10, 11) because a lack of spatial and temporal data necessitates the use of statistical models to understand the role of disturbance and forest structure at these scales.

At the core of all AGB or forest structure maps are field inventory plots (typically  $\leq 1$  ha in size) that are used to estimate forest structural variables (such as tree basal area and height, canopy gaps, and layering). Tree basal area and height are used

in allometric models to estimate AGB and when combined with temporal censuses of the same plots can be used to assess carbon dynamics in forest stands (12). However, to generate landscape-to-regional-scale estimates some studies simply extrapolate plot-based AGB estimates to the total forest area thought to be represented by the plots (13, 14), or they use simple spatial interpolation methods such as kriging (15). Other studies integrate AGB estimates from field plots with remote sensing data to generate landscape and regional estimates of forest AGB and carbon fluxes (6, 16–18). Even as remote sensing data become widely available field plot-based estimates of AGB and structure will remain important for calibrating and validating large-scale remote sensing studies (19, 20).

Regardless of the approach used to estimate forest structure, AGB, or carbon dynamics at landscape and broader scales, an underlying and fundamental assumption is that field plots (*ca.* 1 ha scale) are an unbiased sample of the landscape (*ca.*  $10^2$ - to  $10^4$ -ha scale) (21–23). In the case of Amazonia, fewer than 500 field inventory plots are often used to represent more than  $10^9$  ha of forest (9). However, practical constraints affecting the placement and size of field plots often result in systematic sampling biases (24, 25). These constraints include the physical characteristics and accessibility of the forest, the scientific rationale for the plot, and the labor-intensive nature of field sampling. As landscape-scale heterogeneity increases, plot placement becomes increasingly challenging, and yet it greatly affects whether plot-derived variables are representative of a landscape in question.

Many studies have quantified biases and errors related to the number and size of field plots (26–29), within-plot sampling (30), or a combination of both (21–23, 31). Others have used models

## Significance

Although tropical forests absorb more carbon dioxide as biomass than any other terrestrial ecosystem, biomass estimates disagree substantially at landscape-to-regional scales. Current biomass maps rely upon field plots for extrapolations to larger scales, yet whether field plots accurately represent landscape-scale variables has not been assessed. To our knowledge, this is the first study to compare forest structural variables and aboveground biomass derived from field plots to those derived from their host landscapes using airborne 3D remote sensing. We found that typical field plots can produce substantially biased estimates and the number of plots needed to reduce this bias is impractical, positioning airborne remote sensing as a core tool for mapping forest structure and biomass across tropical landscapes.

Author contributions: D.C.M. and G.P.A. designed research; D.C.M., G.P.A., D.E.K., C.B.A., R.E.M., F.S., and R.T. performed research; D.C.M., G.P.A., D.E.K., C.B.A., and R.E.M. contributed new reagents/analytic tools; D.C.M., G.P.A., D.E.K., C.B.A., and R.E.M. analyzed data; and D.C.M. and G.P.A. wrote the paper.

The authors declare no conflict of interest.

This article is a PNAS Direct Submission.

<sup>1</sup>To whom correspondence should be addressed. Email: dmarvin@carnegiescience.edu.

This article contains supporting information online at [www.pnas.org/lookup/suppl/doi:10.1073/pnas.1412999111/-DCSupplemental](http://www.pnas.org/lookup/suppl/doi:10.1073/pnas.1412999111/-DCSupplemental).

to assess whether existing field-plot networks sufficiently represent forest disturbance dynamics at regional scales (10, 11, 22, 31). However, very few attempts have been made to verify a fundamental assumption that landscape representativeness holds true for field plots in tropical forests, with only two studies conducted in Neotropical forests. Anderson et al. (32) evaluated the sampling bias due to the location of several field plots in the RAINFOR network (33) within *terra firme* and floodplain forest landscapes. By scaling plot-level estimates of AGB to the surrounding landscape weighted by the proportional area of each forest type classified from Landsat images, they found a 3% average bias from five RAINFOR plots in Peru. However, Landsat only provides information on forest cover and, to some extent, forest type, so it is not surprising that a forest plot would well represent a forest landscape in such satellite imagery. In contrast, Chave et al. (21) found about a 10% bias in AGB among field plots in the Panama Canal watershed but relied on data from nearby field plots as the “landscape” for comparison.

Although a few previous studies in the tropics have used remote sensing to develop landscape-scale maps of canopy structure and biomass (e.g., 20, 34–36), no study has assessed whether field plots produce unbiased estimates of these variables at landscape scales. Airborne LiDAR (light detection and ranging) can resolve spatial variation in forest structure, and it can provide high-fidelity biomass estimates at high resolution over the large areas that field plots intend to represent (37). Biases related to spatial scale can thus be uniquely quantified by comparing airborne LiDAR estimates of forest structure and biomass derived from within field-plot boundaries to those from the surrounding host landscape—nearby forest of similar substrate, elevation, and forest type.

We investigated the degree to which typical permanent field plots ( $\leq 1$  ha) accurately represent the forest structure and biomass of their host landscape in Amazonian and Andean forests. The Carnegie Airborne Observatory-2 collected airborne LiDAR data over three distinct forest regions encompassing 10 host landscapes along an elevation gradient in Peru. Four lowland and six montane host landscapes (each *ca.* 500–1,200 ha) were conservatively delimited by similar forest substrates (for lowland regions) or elevation (for montane regions) using LiDAR-derived topographic data (Fig. 1 and Fig. S1). Forest structural variables (tree height, canopy gaps, and layers) and aboveground carbon density (biomass is 48% carbon) were calculated within each field-plot boundary and the surrounding host landscape. All variables were calculated directly from the LiDAR data, isolating the effect of spatial scale between field plot and host landscape under the assumption that airborne LiDAR produces perfectly accurate estimates of each variable (i.e., ignoring any allometric scaling errors). We asked the following questions. (i) How biased are estimates of Amazonian forest structural variables derived from 1-ha field plots compared with those derived throughout their host landscapes? (ii) Are there landscape-scale biases in plot-based estimates of aboveground biomass in Amazonia? (iii) When estimating forest structure and biomass at the landscape scale, what is the error associated with a 1-ha field-plot sampling approach and how many field plots are required to achieve reliably accurate estimates of landscape AGB?

## Results

**Landscape Structure.** In both the lowland Amazon and montane tropical Andes 1-ha field plots often displayed large but highly variable biases in representing forest structure and biomass at a landscape scale (*ca.*  $10^2$ – $10^4$  ha). Even when a forest structural or biomass variable from a field plot approached the mean of its host landscape the landscape probability density distributions of those forest variables were often nonnormally distributed, revealing the difficulty of using a single plot to approximate the surrounding landscape. The high coefficients of variation (CVs)

of these host landscape distributions also reveal substantial landscape-scale heterogeneity (and thus sampling error) for all forest variables presented and summarized here.

Plot-based bias in mean top-of-canopy height (TCH) averaged 11% in lowland and 14% in montane landscapes (Table 1). Mean TCH density distributions of the host landscapes tended to be negatively skewed or multimodal with the exception of one lowland (JEN\_11) landscape and one montane (TRU\_01) landscape (Fig. 2A). The average host landscape CV for mean TCH was moderate at the lowland landscapes (13%) but more than doubled to 28% in the montane landscapes (Table S1).

Field plot-based P:H ratio (i.e., forest canopy architecture, see Methods) estimates showed an average bias of 15% in the lowland landscapes but extreme biases averaging 98% were found in montane landscapes (Table 1). All density distributions of landscape P:H ratio were skewed with the exception of the two lowland erosional *terra firme* (ETF) landscapes (Fig. 2B). The average CV for P:H ratio at the lowland landscapes was 24% but increased substantially to 83% in montane landscapes (Table S1).

The canopy gap size-frequency distribution scaling coefficient  $\lambda$  of the field plots showed moderate bias (9%) in lowland landscapes but increased to 20% throughout the montane landscapes (Table 1). The individual plots tended to have canopy gap  $\lambda$  values near the center of the distributions of their host landscapes (Fig. 2C), with the exception of the three landscapes at the highest elevations. However, the density distributions of  $\lambda$  tended to be nonnormally distributed. The average CV throughout lowland landscapes was 20% but was slightly suppressed at 16% in the montane landscapes (Table S1).

Biases in plot-based canopy gap density (gaps per hectare) were large for both lowland (74%) and montane (64%) landscapes (Table 1). Canopy gap density was not well represented by the field plots for any of the landscapes, and host landscape distributions were positively skewed or multimodal (Fig. 2D). Average CV was very high (100%) for canopy gap density at lowland landscapes and lower but still high (75%) at montane landscapes (Table S1).

Canopy gap size of the field plots also showed large bias for both lowland (47%) and montane (66%) landscapes (Table 1). Host landscape distributions are extremely positively skewed for canopy gap size at all locations except for the two lowland ETF landscapes (Fig. S2). Average CV for canopy gap size was extremely high for both lowland (198%) and montane (160%) landscapes (Table S1).

Maximum TCH, canopy layers, upper canopy gap  $\lambda$ , upper canopy gap density, and upper canopy gap size of the field plots all showed similar patterns of average bias and CV for both lowland and montane landscapes (Tables S2 and S3). Notable exceptions were the smaller bias in field-plot lowland upper canopy gap density (24.1%) and lowland upper canopy gap  $\lambda$  (6.8%). The bias in the number of canopy layers was similar between lowland (29%) and montane (25%) landscapes.

Vertical canopy profiles in the lowland field plots generally tracked those of their host landscapes (Fig. S3 A and B). However, in the montane landscapes the canopy architecture of the field plots strongly biased the representation of forest canopy volume structure to higher canopies than in their host landscapes (Fig. S3C). The downward shift in canopy volume with increasing elevation was not tracked well by the field plots, indicating a bias in any field-plot sampling of montane landscape canopy architecture. This is reflected in the large jump in P:H ratio bias between lowland and montane landscapes.

**Forest Carbon.** LiDAR-estimated aboveground carbon density (EACD) accurately and precisely predicted field plot-based EACD at both lowland and montane locations (Fig. S4). The low bias (2.7 Mg C·ha<sup>-1</sup>) and RMSE (6.0 Mg C·ha<sup>-1</sup>), along with an adjusted  $R^2$  of 0.95, validates the use of universal LiDAR-

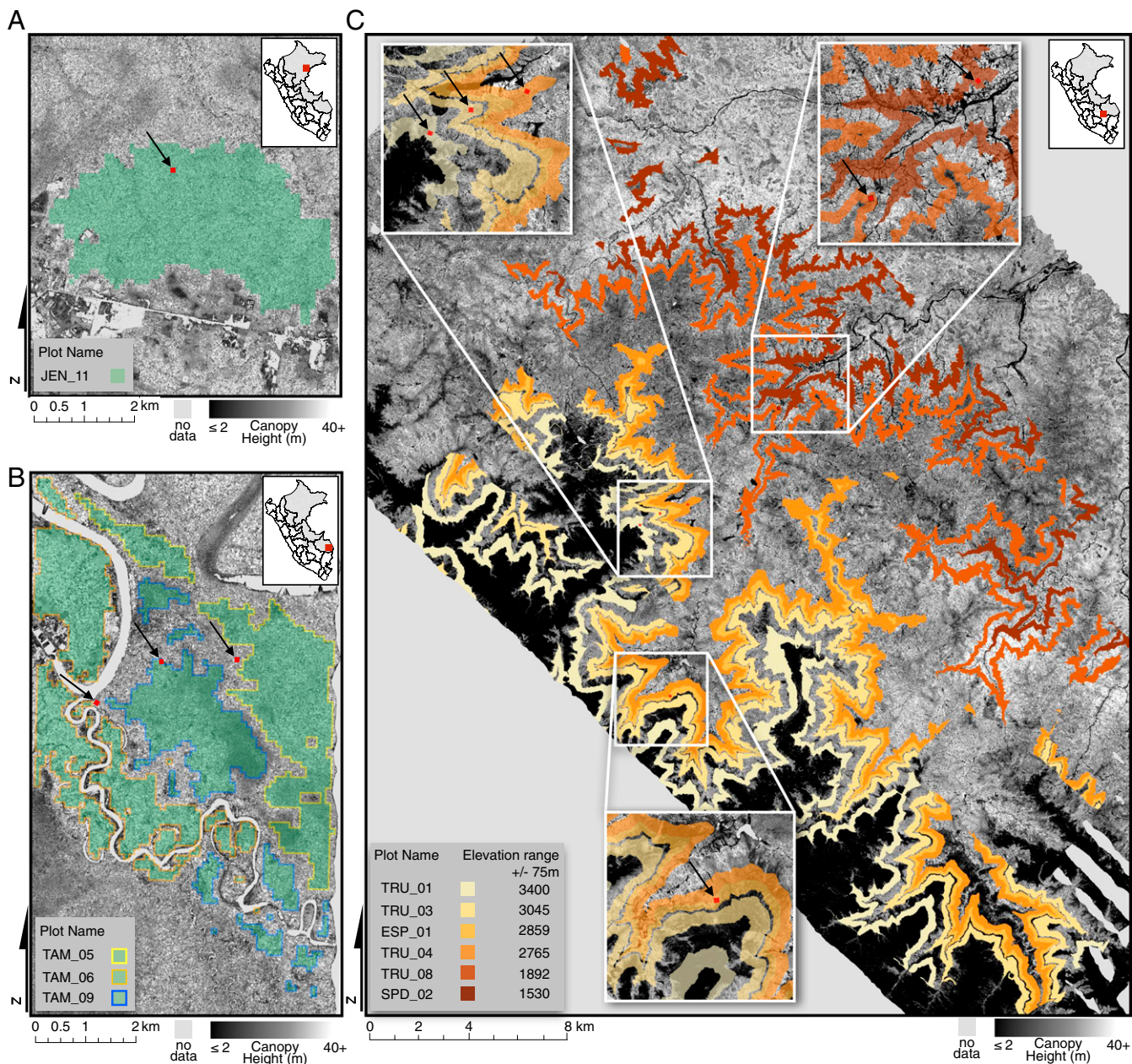


**Fig. 1.** Top-of-canopy height (TCH) showing the three study regions: (A) Jenero Herrera, (B) Tambopata, and (C) Kosñipata in Peru. Descriptive information for each landscape is provided in Table S6. Lowland landscapes are shaded in green and differentiated in B by outlining each host landscape with a different color. Montane landscapes are colored by elevation, with zoom insets for detail using the same scaling as in A and B. The location of the 1-ha field inventory plots is shown in red with black arrows for easier identification. Discontinuities in the montane host landscapes are due to gaps in the LiDAR coverage, whereas discontinuities in the lowland host landscapes result from the narrow elevation ranges used to delineate each forest substrate and the removal of grid cells near water features.

derived EACD (19) across these Andes-to-Amazon landscapes. When EACD was modeled and mapped in each landscape grid cell we found that the field plots rarely represented EACD for each host landscape (Table 2 and Fig. 3A). In fact, all but two plots produced biases  $\geq 10\%$ , and almost always in the direction of overestimating EACD (Table 2 and Fig. 3B). The average CV for the lowland landscapes was 20% and was 32% for the montane landscapes (Table 2). This high heterogeneity can be viewed when EACD is mapped across the lowland landscapes (Fig. 4).

**Landscape Sampling Bias, Error, and Sample Size.** Mean forest structural and biomass values of the landscape grid networks (i.e., 1-ha cells) closely approximated those of the ungridded mean

landscape (Table S4). The only exception was the P:H ratio in both lowland (32% bias) and montane (63% bias), in which all landscape grid networks underestimated the P:H ratio of the host landscape. Mean TCH, canopy gap  $\lambda$ , canopy gap size, and LiDAR EACD biases ranged from 2 to 6% in both lowland and montane landscapes. Canopy layers, upper canopy gap  $\lambda$ , and upper canopy gap size also showed low to moderate biases (Table S4). Average CV values for the grid networks were 10% or greater for all variables at both lowland and montane landscapes (Tables S1 and S3).

On average, a total of 44 lowland and more than 85 montane 1-ha field plots are needed to reliably (i.e., a probability of 0.9) estimate EACD to within 90% of the actual landscape mean value (Fig. 5B and Table S5). To achieve an estimate that is 95%

**Table 1.** Mean values of forest structural variables for each field plot and associated host landscape grid network

Plot	Substrate	Mean TCH, m				P:H ratio				Canopy gap $\lambda$				Canopy gap density, gaps per hectare				Canopy gap size, m <sup>2</sup>				
		Grid network		%Δ, %	Plot	Grid network		%Δ, %	Plot	Grid network		%Δ, %	Plot	Grid network		%Δ, %	Plot	Grid network		%Δ, %	Plot	
		Plot	network	Plot	network	Plot	network	Plot	network	Plot	network	Plot	network	Plot	network	Plot	network	Plot	network	Plot	network	
<b>Lowland</b>																						
JEN_11	ETF	22.9	22.6	1.7	0.66	0.60	11.4	1.72	1.94	-11.7	9.0	4.0	123.5	4.4	3.7	21.2						
TAM_06	DFP	25.5	22.0	15.6	0.59	0.47	25.9	1.61	1.86	-13.4	5.0	6.5	-23.1	3.4	19.2	-82.3						
TAM_09	DFP	20.9	18.8	11.4	0.47	0.52	-10.1	1.98	2.03	-2.4	8.0	4.2	89.1	2.6	6.1	-57.1						
TAM_05	ETF	23.5	20.2	16.3	0.61	0.55	11.0	1.88	2.04	-7.7	2.0	4.9	-59.1	2.5	3.4	-27.0						
Average bias				11.3			14.6			8.8			73.7			46.9						
<b>Montane</b>																						
SPD_02	Montane	20.2	16.0	26.1	0.42	0.24	78.7	NA	1.77	NA	0.0	20.1	-100.0	NA	20.5	NA						
TRU_08	Montane	12.5	13.8	-8.9	0.44	0.19	125.9	1.75	1.79	-2.1	5.0	24.2	-79.3	3.4	13.8	-75.3						
TRU_04	Montane	14.5	12.6	15.4	0.62	0.21	197.4	1.78	1.88	-5.3	3.0	31.1	-90.4	3.0	8.7	-65.6						
ESP_01	Montane	13.4	12.0	11.6	0.48	0.21	136.0	2.93	1.88	55.7	13.0	30.4	-57.3	1.4	11.1	-87.5						
TRU_03	Montane	10.9	11.4	-4.7	0.12	0.19	-38.8	2.56	1.87	36.6	26.0	31.1	-16.5	1.5	13.4	-88.8						
TRU_01	Montane	10.3	9.0	14.1	0.13	0.15	-12.7	2.17	1.81	19.6	25.0	42.0	-40.5	3.5	17.9	-80.6						
Average bias				13.5			98.2			19.9			64.0			66.3						

%Δ is the difference between the plot and grid network estimates as a percentage of the grid network. Average bias is the average absolute percent bias. Canopy gap-related variables are derived from gaps at vegetation height  $\leq 2$  m.  $\lambda$ , size-frequency distribution scaling coefficient; NA, not applicable; P:H ratio, ratio of forest canopy architecture; TCH, top-of-canopy height.

accurate, those amounts increased to an average of more than 85 field plots per lowland and more than 100 field plots per montane landscape (Fig. 5*A* and **Table S5**). At a lower (80%) threshold accuracy, an average of 12 field plots and 27 field plots are needed per lowland and montane landscapes, respectively (Fig. 5*C*). The most homogenous landscape (JEN\_11) with a CV of 9.5% for EACD requires 10 1-ha field plots to estimate its host landscape EACD to an accuracy of 90%. For more heterogeneous landscapes such as TRU\_08 (EACD CV of 38.1%) over 100 1-ha field plots are needed to estimate its host landscape EACD to an accuracy of 90%.

## Discussion

Forest science is increasingly being called upon to provide accurate, large-scale estimates of tropical forest carbon stocks and structure for use in conservation and resource policy development and for understanding ecosystem function and change over time. Field plots are used, sometimes in combination with remote sensing data, to produce these estimates. Using airborne LiDAR to compare forest structural variables and aboveground biomass derived from field plots to those derived from their host landscapes, we found substantial biases (9–98%) in field-plot data that should restrict their use in extrapolations to landscape scales. These biases were present in both lowland Amazonian and montane Andean landscapes and were found across all forest variables measured.

The largest biases were found in the number and size of forest canopy gaps (47–74%), which are direct expressions of tree mortality, damage, and regrowth and play integral roles in plant community structure and forest carbon storage (3, 38, 39). Our results suggest that the use of canopy gap data from field plots is invalid for drawing conclusions of landscape-scale canopy gap processes. Although not as severe, the size and directionality of bias in canopy gap  $\lambda$  (9% lowland vs. 20% montane) may nonetheless result in incorrect interpretations about the size of disturbance events in lowland and montane landscapes. Thus, field plot-based estimates of canopy gap-size frequency distributions likely will lead to erroneous estimates of forest carbon loss via disturbance (40).

We found that aboveground carbon stocks are often systematically overestimated—by as much as 29% in montane and 26% in lowland forests—using field plots compared with the landscapes

hosting those plots. A recent synthesis of biomass estimates from tropical montane forest plots concluded that these forests hold a substantial and widely unrecognized amount of carbon (41). The highly heterogeneous distribution of carbon within host landscapes (Fig. 4) illustrates the difficulty in extrapolating individual 1-ha estimates to larger scales. This underscores the challenge and major limitations of using field plots as “truth” in comparisons with remote sensed-assisted maps of forest carbon stocks (9).

The average bias of each forest structural variable yields a general understanding of how field plots represent the landscape. However, examining where an individual field plot falls inside the host landscape distribution often reveals further bias. Individual field plots can approximate the mean value of the host landscape, and when the distribution of that landscape-level variable is normal a 1-ha field plot can serve as a viable representative (e.g., JEN\_11 in Fig. 2*A*). However, the distribution of most forest structural properties, as well as biomass, is often nonnormal with skewed or multimodal distributions. As a result, a large number of field plots would be required to capture the heterogeneity in a statistically robust way.

There are numerous points at which bias or error can be introduced to field-plot estimates of forest structure and biomass (reviewed in ref. 24). By comparing the LiDAR data in the locations of 1-ha field plots to their host landscapes we limited our assessment of bias solely to that resulting from plot-to-landscape scaling. Consequently, we can neither draw conclusions about unrepresented forest types in the Amazon basin nor extend our analysis beyond the landscape scale. Although such analyses are needed, they fall outside the scope of this paper.

We do not criticize the effort expended in creating and maintaining field-plot networks or the value of the data gathered from them. All of the plots used in the current study were created for a variety of reasons other than scaling biomass or structural estimates to the landscape and/or region. Our understanding of local forest processes across a range of environmental and floristic gradients have been greatly advanced by such plot networks (42–44). However, our results make clear that accurate estimates of landscape-scale forest properties and processes cannot readily be obtained from plots. Therefore, we must develop new sampling approaches that minimize plot bias or, at the very least, better account for the biases of current plots.

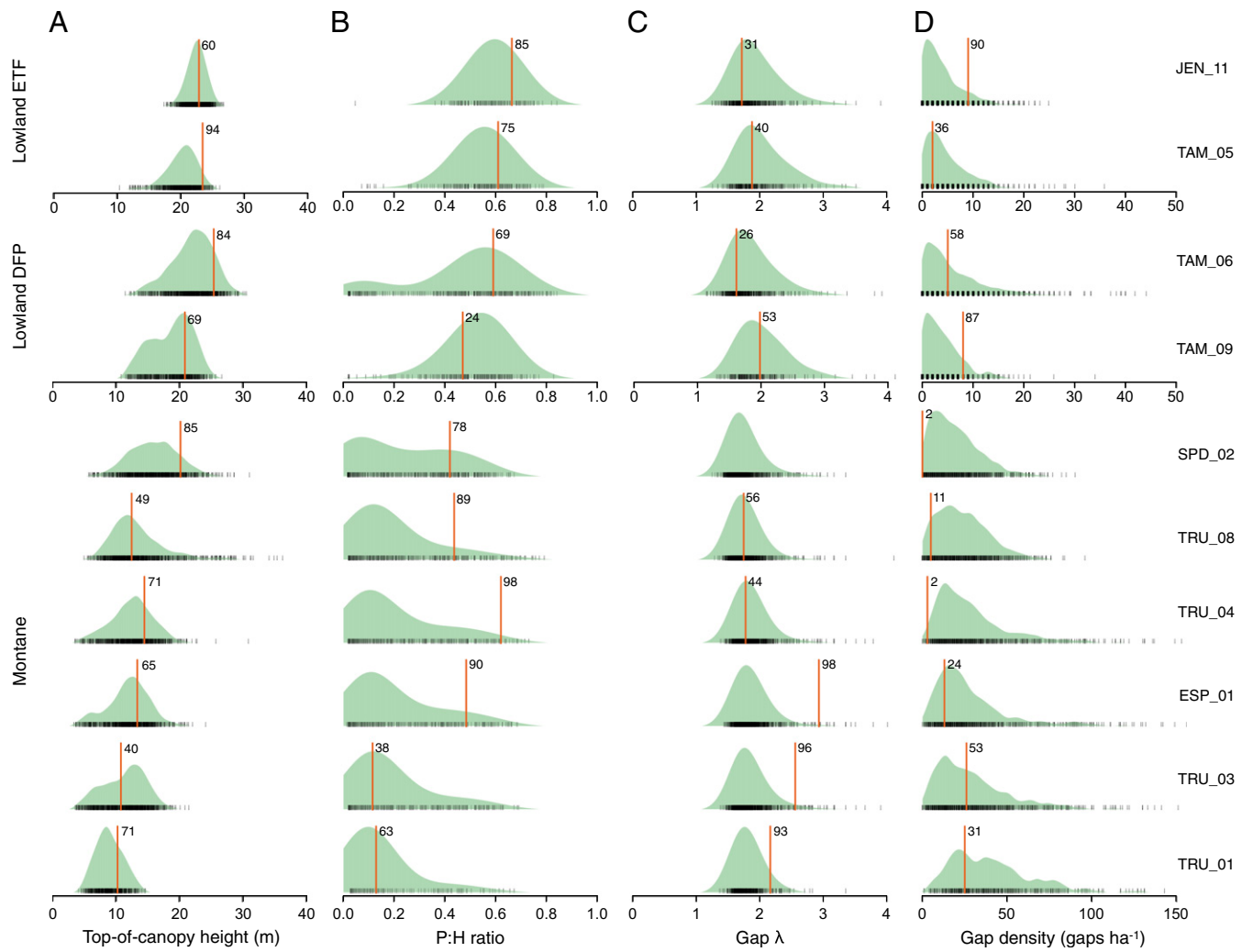


**Fig. 2.** Probability density distributions of (A) top-of-canopy height (TCH), (B) P:H ratio, (C) canopy gap  $\lambda$  (vegetation height  $\leq 2$  m), and (D) canopy gap density (vegetation height  $\leq 2$  m) across landscape grid networks (green), with individual grid cells plotted as small black vertical lines. Red lines are the mean values from the field plots, with adjacent numbers indicating the percentile rank within the landscape grid network (determined from the empirical cumulative distribution function). Montane plots are ordered by increasing elevation. The absence of canopy gaps in SPD\_02 means no field-plot canopy gap  $\lambda$  can be calculated. Note the different axes between lowland and montane landscapes in D. Canopy gap size is presented in Fig. S2.

The central issue is how to accurately characterize heterogeneous tropical forest landscapes. Characterization of landscape or regional forest heterogeneity is not possible without using some means of remote sensing data at these scales. Using active remote-sensing instruments (i.e., LiDAR and radar) able to resolve heterogeneity in forest structural attributes within landscapes is essential. Once a basic understanding of a landscape's spatial heterogeneity is developed from airborne or satellite data, multiple field sampling plots might be placed such that the full range of landscape variability is captured. In this case, multiple plots ( $\leq 1$  ha) are recommended rather than one large plot to avoid spatial autocorrelation effects (25). However, average CV values calculated in this study were greater than 20% for most variables (Table 2 and Tables S1 and S3), indicating high spatial sampling error regardless of where plots are placed within the landscape (23).

The inherently high spatial sampling error of Amazonian landscapes indicates that a large number of field plots are required to achieve reliably high accuracy in estimating forest structure and biomass variables. Our field-plot sample size simulations for EACD reveal that even a relatively homogenous landscape (CV of 9.5%) would require 10 randomly placed 1-ha

field plots to achieve 90% accuracy in estimating the landscape mean EACD (Fig. 5B and Table S5). As landscape heterogeneity increases the number of field plots required to achieve 90% accuracy balloons to over 100 plots per landscape. On average in both lowland and montane landscapes an impractical number of field plots per landscape (44 per lowland and  $>85$  per montane) are needed to achieve 90% accuracy, whereas a higher level of accuracy (95%) requires nearly double the number of plots in many cases (Table S5). Under a reduced emissions from deforestation and degradation (REDD+) program, increasing uncertainty in forest carbon estimates leads to a decreasing monetary value of forest carbon (45–47), with some studies suggesting that accuracies below 95% could exclude (or greatly reduce) most nations from generating monetary benefits under an REDD+ program (48, 49).

The spatial biases and errors inherent in field-plot sampling of heterogeneous landscapes necessitate an alternative approach. Future studies of forest structure and biomass could use airborne LiDAR as the primary sampling technique to fully resolve landscape structural variables. Because no spaceborne LiDAR is currently operating, only airborne LiDAR can feasibly provide the necessary continuous spatial coverage to fully capture

**Table 2.** Comparison of plot and grid network mean LiDAR EACD for each landscape

Mean LiDAR EACD, Mg C·ha <sup>-1</sup>					
Plot	Forest	Plot	Grid network	%Δ, %	CV, %
<b>Lowland</b>					
JEN_11	ETF	118.1	115.4	2.4	9.5
TAM_06	DFP	111.7	89.6	24.7	24.2
TAM_09	DFP	81.4	69.8	16.6	27.1
TAM_05	ETF	98.2	77.7	26.3	18.7
				Average bias 17.5	Average CV 19.9
<b>Montane</b>					
SPD_02	Montane	98.7	76.7	28.6	27.4
TRU_08	Montane	58.4	65.6	-9.7	38.1
TRU_04	Montane	68.9	58.7	17.4	31.3
ESP_01	Montane	63.1	55.9	12.9	32.0
TRU_03	Montane	49.5	52.5	-5.7	34.1
TRU_01	Montane	46.7	40.2	16.2	27.7
				Average bias 18.5	Average CV 31.8

%Δ is the difference between the plot and grid network estimates as a percentage of the grid network. CV is coefficient of variation of the grid network. Average bias is the average absolute percent bias. EACD, estimated aboveground carbon density.

landscape heterogeneity, allowing for accurate assessments of forest structure and carbon stocks. Advances in flight planning, collection of LiDAR data, and scaling have reduced costs enormously, approaching \$0.01·ha<sup>-1</sup> in some regions (16, 50). Sampling landscapes with field plots cannot achieve the same economies of scale as airborne LiDAR because plot-level costs increase on a per-area basis. Plot-based sampling of the 10 landscapes in this study would require more than 700 1-ha field plots to achieve a reliably accurate estimate (Table S5). Such a strategy is unfeasible and unproductive, yielding fewer than 9,000 ha of tropical forest carbon stock estimates. When studying forest structure and carbon at landscape or regional scales, field plots can be used for calibration and validation of remote sensing data and for understanding local-scale controls on forest structure and carbon.

We have entered an era in which extrapolations and predictions of forest properties based on sparsely and/or nonrandomly distributed field plots are no longer acceptable for understanding tropical forests in regional or global carbon cycles. Reducing uncertainties to a level just acceptable enough to pass peer review only undermines the goals of tropical biodiversity conservation and climate-change mitigation. Moreover, there are considerable monetary benefits to reducing uncertainties as the creation and price of carbon credits under REDD+ are linked to the accuracy of forest carbon estimates (45, 49). Fortunately, continuing technological, theoretical, and analytical advancements offer the potential for limiting biases and reducing uncertainties in pursuit of these goals. If ecologists are to effectively embrace the shift toward investigations at meso- to macroscales (51, 52) a fundamental shift in the way we approach field sampling must occur. We have shown here that the status quo is unacceptable if high accuracy across large spatial scales is to be achieved.

## Methods

**Study Landscapes.** We selected three tropical forest landscapes in Peru: one northern lowland in Jenaro Herrera, one southern lowland in Tambopata, and one montane in the Kosñipata Valley (Table S6). From among these areas we defined 10 local host landscapes (*Landscape Sampling Area*), each of which is associated with a 1-ha permanent field plot used for forest inventories by the RAINFOR and Andes Biodiversity and Ecosystem Research Group (ABERG) plot networks (33, 53). In the lowland landscapes mean annual precipitation ranges from 2,600 to 2,700 mm and mean annual temperature from 24.0 to 26.6 °C. In the montane landscapes, mean annual precipitation ranges from 1,705 to 4,628 mm and mean annual temperature varies from 8.0 °C at the highest elevation to 18.5 °C at lower submontane elevations. The forest substrates in the lowland landscapes fall into two broad classes: ETF substrates on elevated terraces containing soils with high clay content classified as Ultisols and depositional floodplain (DFP) substrates in low-lying areas near rivers and streams with loamy-to-sandy soils classified as Inceptisols (54). The montane landscapes are on substrates with soils classified as Inceptisols or Entisols (55).

**Airborne LiDAR Collection and Layer Processing.** The LiDAR data were collected in August 2011 using the Carnegie Airborne Observatory-2 Airborne Taxonomic Mapping System (AToMS), which is carried onboard a twin turbopropeller Dornier 228 aircraft (56). The AToMS LiDAR is a dual-laser, scanning waveform system capable of operating at 500,000 laser shots per second. For this data collection, the aircraft was operated at speeds of up to 110 kn at an altitude averaging 2,000 m above ground level. The LiDAR settings were maintained at an average on-the-ground laser spot spacing of

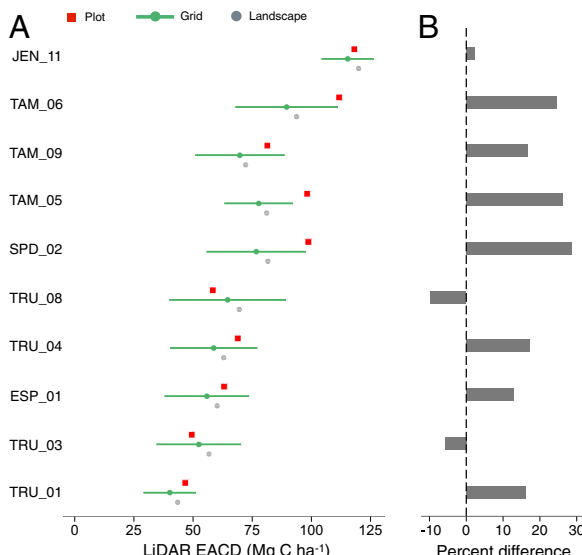


**Fig. 3.** (A) LiDAR estimated aboveground carbon density (EACD) at the plot (red square), grid network (green circle), and landscape (gray circle) level for each location. Green bars show the SD in EACD for the grid network. (B) Errors are represented as the difference between the field plot EACD and the grid network EACD as a percentage of the grid network EACD.

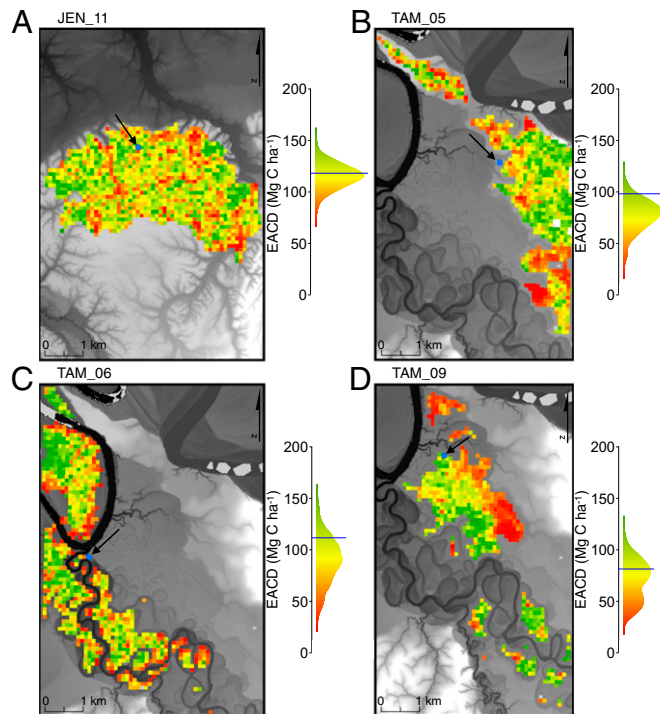


**Fig. 4.** Maps of estimated aboveground carbon density (EACD) with color scheme from dark red (low EACD) to dark green (high EACD) matching the distribution plots to the right for lowland landscapes (A) JEN\_11, (B) TAM\_05, (C) TAM\_06, and (D) TAM\_09. Map background is a digital elevation model with shading as in Fig. S1 and field-plot locations are represented by a blue square in each map with black arrows for easier identification. EACD probability density distributions of the lowland host landscape grid networks are plotted to the right of each map, with the blue line representing the mean EACD from the associated 1-ha field inventory RAINFOR plot. The three Tambopata host landscapes (TAM\_05, TAM\_06, and TAM\_09) are the same as in Fig. 1B but shown here in separate figure windows for clarity.

two shots per square meter, peaking at four shots per square meter in areas of flightline overlap. This level of sampling ensured that the derived LiDAR measurements were highly precise in horizontal and vertical space (56).

Following data acquisition, laser ranges from the LiDAR were combined with embedded high-resolution Global Positioning System–Inertial Measurement Unit (GPS–IMU) data to determine the 3D locations of laser returns, producing a “cloud” of LiDAR data. The LiDAR data cloud consists of a very large number of georeferenced point elevation estimates (centimeters), relative to a reference ellipsoid (WGS 1984). LiDAR data points were processed to identify which laser pulses penetrated the canopy volume and reached the ground surface. We used these points to interpolate a raster digital terrain model (DTM) for the ground surface. This was achieved using a 5- × 5-m kernel passed over each flight block; the lowest elevation estimate in each kernel was assumed to be ground. Subsequent points were evaluated by fitting a horizontal plane to each of the ground seed points. If the closest unclassified point was <5.5° and <1.5 m higher in elevation it was classified as ground. This process was repeated until all points within the block were evaluated. The digital surface model (DSM) was based on interpolations of all first-return points. Measurement of the vertical difference between the DTM and DSM yielded a model of TCH.

Gaps in the canopy were defined by applying the definition of Brokaw (57) to the TCH model. Openings in the forest canopy extending down to a vegetation height of ≤2 m and to a vegetation height of ≤20 m were used as gap thresholds. The former can be thought of as whole-tree and large canopy branch failures (“canopy gaps”), whereas the latter can be considered crown and branch failures in the upper canopy (54). Upper canopy gaps were not computed for the montane landscapes.

The vertical distribution of LiDAR points was processed by binning the data into volumetric pixels (voxels) at 5- × 5-m spatial and 1-m vertical resolution (58). The DTM was used to standardize the vertical datum of each voxel.

Therefore, the heights of each vertical “slice” of a vegetation canopy were defined relative to the ground at the horizontal center of each voxel. After all LiDAR points were binned in the volume cube, each vertical column of the cube was divided by the total number of LiDAR points in that column, yielding the percentage of LiDAR points that occurred in each voxel. This approach has the advantage of decreasing our sensitivity to localized variations in canopy leaf density or tree branch characteristics, which can result in a different number of LiDAR returns from voxel to voxel. It is important to note that our vertical profiles are based on LiDAR returns that serve as proxies for actual vertical canopy profiles (58, 59).

**LiDAR-Derived Structural Variables.** We calculated both the mean and maximum TCH per unit area. Using the slicer layers, we computed a ratio of height above ground at the maximum canopy volume ( $P$ ) to the 99th percentile of total canopy height ( $H$ ). The  $P:H$  ratio is a metric describing the architecture of a forest canopy over a given area (60). We determined the number of canopy layers by taking the first derivative of the vertical profile and summing the number of negative-to-positive sign changes.

We computed the gap size-frequency variable  $\lambda$  for both the ≤2-m vegetation height (canopy gap) and ≤20-m vegetation height (upper canopy gap) layers. We used the approach and R syntax provided by ref. 54, where the gap size-frequency distribution of a given area was quantified using the zeta distribution. For the zeta distribution with parameter  $\lambda$ , the probability that gap size takes the value  $k$  is

$$f(k) = \frac{k^{-\lambda}}{\zeta(\lambda)}, \quad [1]$$

where the denominator is the Riemann zeta function and is undefined for  $\lambda = 1$ . This distribution is also known as the “discrete Pareto distribution” and is appropriate for modeling the size-frequency of canopy gaps (hereafter referred to as “gap  $\lambda$ ”) (31, 61, 62). We calculated the gap density (gaps per hectare) and the average gap size per unit area for both the canopy gap and upper canopy gap layers.

Instead of AGB, we calculate aboveground carbon density (carbon is 48% of dry woody biomass; 63). EACD was calculated from the LiDAR-derived TCH layer using the plot-aggregate allometric equation from ref. 19:

$$EACD_{\text{LiDAR}} = aTCH^{b_1} BA^{b_2} p_{BA}^{b_3}, \quad [2]$$

where TCH is the mean LiDAR-derived top-of-canopy height for the sample area, and  $a$ ,  $b_1$ ,  $b_2$ , and  $b_3$  are universal model regression coefficients (from table 2 in ref. 19). BA is TCH-estimated basal area, and  $p_{BA}$  is TCH-estimated basal-area weighted wood density, of the form

$$BA = m_1 TCH + b_1, \quad [3]$$

$$p_{BA} = m_2 TCH + b_2, \quad [4]$$

where  $m_1$ ,  $m_2$ ,  $b_1$ , and  $b_2$  are regression coefficients specific to the subregion of Peru where each plot is located (from table 3 in ref. 19). Note that this plot-level allometric equation was developed from a global network of 904 tropical field inventory plots (used for calibration/validation of remote sensing data) incorporating a wide range of forest physiognomies, floristics, soils, and environmental variables.

**Landscape Sampling Area.** We introduce the concept of a “host landscape,” or the surrounding forest within ~10<sup>2</sup>–10<sup>4</sup> ha of a field plot that contains similar substrate, elevation, and forest type. For each host landscape we first defined the maximum host landscape sampling area (polygon) based on a set of criteria unique to each elevation and forest substrate combination (Fig. 1 and Fig. S1). To differentiate lowland DFP from lowland ETF landscapes, elevation breakpoints between each substrate were found by manually examining each lowland DEM and creating masks based on these breakpoints. A 50-m inward buffer was applied to each mask to ensure there was no overlap with adjacent landscape types.

For montane landscapes, we created a 75-m buffer up and down slope from the centroid of each field plot. This buffer distance allowed the creation of nonoverlapping polygon “bands” (Fig. 1C and Fig. S1C) from which we could sample the host landscapes of similar elevation, except in the case of ESP\_01 and TRU\_04, which had a 56-m overlap. These polygon bands were created from the full extent of the LiDAR sampling area for the Kosñipata landscape.

We gridded each host landscape polygon into 100- × 100-m cells to form a grid network used to create a 1-ha sampling distribution of the host landscape. We removed grid cells that overlapped water features by more

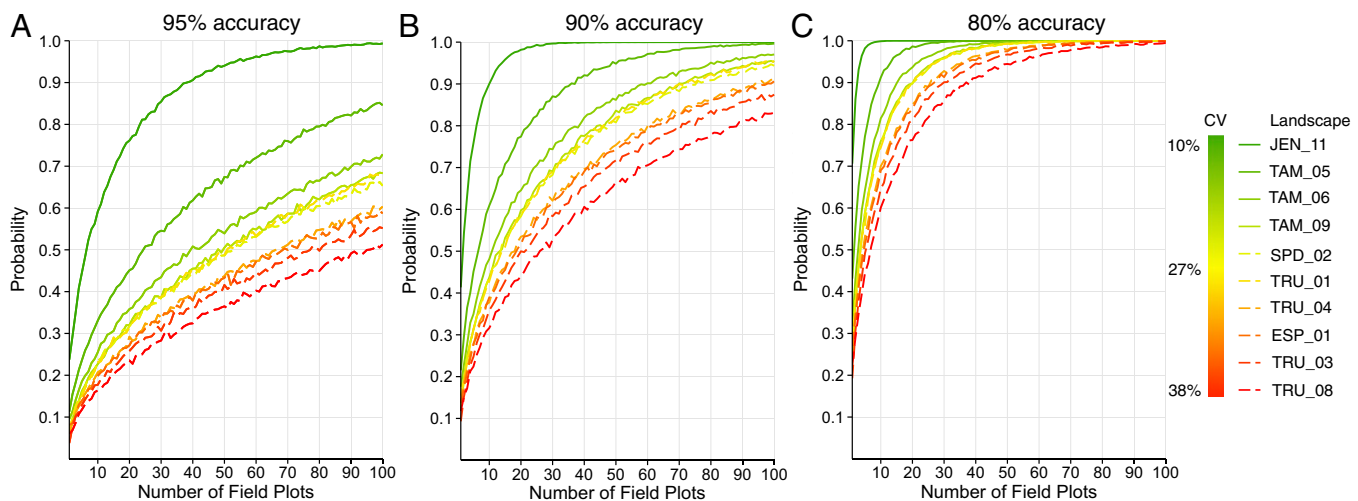


**Fig. 5.** Simulation results showing the number of 1-ha field plots needed to reach a certain probability of estimating the mean estimated aboveground carbon density (EACD) of each landscape to within (A) 95% accuracy, (B) 90% accuracy, and (C) 80% accuracy. Line colors represent the CV of the landscape grid network. Solid lines denote lowland landscapes and dashed lines denote montane landscapes.

than 0.25 ha. To identify zones of land use, landslides, nonforested areas above the tree line, water bodies, and other anomalous landscape features to remove from the grid network we created a mask using sliver bands that contained no LiDAR returns from 15–45 m and 5–30 m in height for lowland and montane host landscape, respectively. A low-pass Gaussian filter with a 15-m kernel and a median filter with a 3-m kernel were used to smooth the masks for the lowland and montane landscapes, respectively. These masks were visually compared with each host landscape TCH layer and grid cells overlapping anomalous landscape features by more than 0.25 ha were manually selected for removal. In the one case where the maximum sample areas overlapped (TRU\_04 and ESP\_01), any grid cells that fell into the other host landscape were removed from the grid network. The total gridded area (or number of grid cells) of each landscape is shown in Table S6.

Coordinates of the field plots were collected using a survey-grade GPS with multiple-bounce filtering and postdifferential correction with average uncertainties of  $\leq 2$  m (Leica GS-50+; Leica Geosystems Inc.). All image processing, data extraction, and vector layer creation was performed in IDL/ENVI (Exelis) and/or ArcGIS (Esri).

**Analysis.** Data for each LiDAR-derived structural variable was extracted and analyzed at three spatial scales for each host landscape: the 1-ha field plot, the 1-ha grid network, and the full ungridded landscape. For the purposes of this study we assume that airborne LiDAR produces perfectly accurate estimates of each variable (i.e., excluding allometric scaling/measurement errors). This allows for the isolation of the effect of spatial scale between field plot and host landscape. The difference between a field plot and the mean of its host grid network was calculated as a percent of the host grid network's mean. We use the mean even when a grid network's distribution is skewed or multimodal because the grid network is the full population, rather than a population sample that would require a different measure of central tendency. A sample (collection of field plots) is biased if its estimate of the population (collection of host landscapes) is different from the true value of the population (64). To assess the plot-level bias, for each set of lowland and montane host landscapes we calculate bias as the average of the absolute value of the percent differences between each individual plot and associated grid network. To assess the inherent bias in a 1-ha sampling approach regardless of plot placement, for each set of lowland and montane

host landscapes we calculate bias as the average of the absolute value of the percent differences between each grid network and its ungridded landscape.

To characterize spatial heterogeneity we calculated the CV for each forest structural variable as

$$CV = \frac{\sigma}{\mu} \times 100, \quad [5]$$

where  $\sigma$  is the SD and  $\mu$  is the mean of the variable at a particular spatial scale (i.e., field plot, grid network, or ungridded landscape). Sampling error is the unpredictable variation (heterogeneity) that would be accounted for if the entire population could be sampled. Therefore, we also use the CV to quantify spatial sampling error (25).

We used Monte Carlo simulations to determine how many field plots are needed to estimate the mean EACD value of a landscape to a specified accuracy. For each landscape, a random sample of 1-ha grid cells was selected from the landscape grid and the sample mean compared with the mean of the full landscape grid. This was repeated 10,000 times to find the probability that the selected number of field plots was accurate to within 95, 90, and 80% of the mean of the full landscape grid. We ran this simulation for sample sizes of 1 through 100 1-ha field plots.

To assess the accuracy and precision of using TCH to predict EACD, we regressed LiDAR-based EACD against field plot-derived EACD obtained from recent published values (43, 65, 66). Using Eqs. 2–4, we modeled EACD using mean TCH for each field plot, and for each cell in the grid networks. We assessed bias and CV as above and mapped EACD across each lowland grid network. All data processing and analyses were performed in R (67).

**ACKNOWLEDGMENTS.** We thank N. Vaughn for assistance with processing the LiDAR data, and M. Silman and two anonymous reviewers for providing comments that greatly improved the manuscript. This study was supported by the John D. and Catherine T. MacArthur Foundation. The Carnegie Airborne Observatory is made possible by the Gordon and Betty Moore Foundation, the John D. and Catherine T. MacArthur Foundation, Avatar Alliance Foundation, W. M. Keck Foundation, the Margaret A. Cargill Foundation, Grantham Foundation for the Protection of the Environment, Mary Anne Nyburg Baker and G. Leonard Baker Jr., and William R. Hearst III.

1. Asner GP, Wessman CA, Archer S (1998) Scale dependence of absorption of photosynthetically active radiation in terrestrial ecosystems. *Ecol Appl* 8(4): 1003–1021.
2. Brokaw N (1985) Treefalls, regrowth, and community structure in tropical forests. *The Ecology of Natural Disturbance and Patch Dynamics*, eds Picket STA, White PS (Academic, Washington, DC), pp 53–69.
3. Hubbell SP, Foster RB (1986) Canopy gaps and the dynamics of a neotropical forest. *Plant Ecology*, ed Crawley MJ (Blackwell, Oxford), pp 77–95.
4. Pan Y, et al. (2011) A large and persistent carbon sink in the world's forests. *Science* 333(6045):988–993.
5. UNFCCC (2011) *A Sourcebook of Methods and Procedures for Monitoring and Reporting Anthropogenic Greenhouse Gas Emissions and Removals Caused by Deforestation, Gains and Losses of Carbon Stocks in Remaining Forests, and Forestation* (GOFC-GOLD, Natural Resources Canada, Alberta, Canada).
6. Harris NL, et al. (2012) Baseline map of carbon emissions from deforestation in tropical regions. *Science* 336(6088):1573–1576.
7. Houghton RA, Lawrence KT, Hackler JL, Brown S (2001) The spatial distribution of forest biomass in the Brazilian Amazon: A comparison of estimates. *Glob Change Biol* 7(7):731–746.
8. Mitchard ET, et al. (2013) Uncertainty in the spatial distribution of tropical forest biomass: A comparison of pan-tropical maps. *Carbon Balance Manag* 8(1):10.
9. Mitchard ETA, et al. (2014) Markedly divergent estimates of Amazon forest carbon density from ground plots and satellites. *Glob Ecol Biogeogr* 23(8): 935–946.

10. Chambers JQ, Negron-Juarez RI, Hurt G, Marra DM, Higuchi N (2009) Lack of intermediate-scale disturbance data prevents robust extrapolation of plot-level tree mortality rates for old-growth tropical forests. *Ecol Lett* 12(12):E22–E25.
11. Lloyd J, Gloor EU, Lewis SL (2009) Are the dynamics of tropical forests dominated by large and rare disturbance events? *Ecol Lett* 12(12):E19–E21, discussion E22–E25.
12. Phillips OL, et al. (2009) Drought sensitivity of the Amazon rainforest. *Science* 323(5919):1344–1347.
13. Fearnside PM (1997) Greenhouse gases from deforestation in Brazilian Amazonia: Net committed emissions. *Clim Change* 35(3):321–360.
14. FAO (Food and Agriculture Organization) (2010) *Global Forest Resources Assessment 2010* (Food and Agriculture Organization of the United Nations, Rome).
15. Malhi Y, et al. (2006) The regional variation of aboveground live biomass in old-growth Amazonian forests. *Glob Change Biol* 12(7):1107–1138.
16. Asner GP, et al. (2010) High-resolution forest carbon stocks and emissions in the Amazon. *Proc Natl Acad Sci USA* 107(38):16738–16742.
17. Baccini A, et al. (2012) Estimated carbon dioxide emissions from tropical deforestation improved by carbon-density maps. *Nat Clim Chang* 2:182–185.
18. Saatchi SS, et al. (2011) Benchmark map of forest carbon stocks in tropical regions across three continents. *Proc Natl Acad Sci USA* 108(24):9899–9904.
19. Asner GP, Mascaro J (2014) Mapping tropical forest carbon: Calibrating plot estimates to a simple LiDAR metric. *Remote Sens Environ* 140:614–624.
20. Drake J, et al. (2003) Above-ground biomass estimation in closed canopy Neotropical forests using lidar remote sensing: Factors affecting the generality of relationships. *Glob Ecol Biogeogr* 12(2):147–159.
21. Chave J, et al. (2004) Error propagation and scaling for tropical forest biomass estimates. *Philos Trans R Soc Lond B Biol Sci* 359(1443):409–420.
22. Gloor M, et al. (2009) Does the disturbance hypothesis explain the biomass increase in basin-wide Amazon forest plot data? *Glob Change Biol* 15(10):2418–2430.
23. Muller-Landau HC, Dette M, Chisholm RA, Hubbell SP, Condit R (2014) Detecting and projecting changes in forest biomass from plot data. *Forests and Global Change*, eds Coomes DA, Burslem DFRP, Simonson WD (Cambridge Univ Press, Cambridge, UK), pp 1–35.
24. Clark DB, Kellner JR (2012) Tropical forest biomass estimation and the fallacy of misplaced concreteness. *J Veg Sci* 23(6):1191–1196.
25. Réjou-Méchain M, et al. (2014) Local spatial structure of forest biomass and its consequences for remote sensing of carbon stocks. *Biogeosciences Discuss* 11:5711–5742.
26. Keller M, Palace M, Hurt G (2001) Biomass estimation in the Tapajos National Forest, Brazil: Examination of sampling and allometric uncertainties. *For Ecol Manage* 154(3):371–382.
27. Chave J, et al. (2003) Spatial and temporal variation of biomass in a tropical forest: Results from a large census plot in Panama. *J Ecol* 91(2):240–252.
28. Chambers JQ, et al. (2004) Response of tree biomass and wood litter to disturbance in a Central Amazon forest. *Oecologia* 141(4):596–611.
29. Baraloto C, et al. (2013) Rapid simultaneous estimation of aboveground biomass and tree diversity across neotropical forests: A comparison of field inventory methods. *Biotropica* 45(3):288–298.
30. Phillips OL, et al. (2002) Changes in growth of tropical forests: Evaluating potential biases. *Ecol Appl* 12(2):576–587.
31. Fisher JI, Hurt G, Thomas RQ, Chambers JQ (2008) Clustered disturbances lead to bias in large-scale estimates based on forest sample plots. *Ecol Lett* 11(6):554–563.
32. Anderson LO, et al. (2009) Influence of landscape heterogeneity on spatial patterns of wood productivity, wood specific density and above ground biomass in Amazonia. *Biogeosciences* 6:1883–1902.
33. Peacock J, Baker TR, Lewis SL, Lopez Gonzalez G, Phillips OL (2007) The RAINFOR database: Monitoring forest biomass and dynamics. *J Veg Sci* 18(4):535–542.
34. Drake JB, et al. (2002) Estimation of tropical forest structural characteristics using large-footprint lidar. *Remote Sens Environ* 79(2–3):305–319.
35. Saatchi S, Marlier M, Chazdon RL, Clark DB, Russell AE (2011) Impact of spatial variability of tropical forest structure on radar estimation of aboveground biomass. *Remote Sens Environ* 115(11):2836–2849.
36. Clark ML, Roberts DA, Ewel JJ, Clark DB (2011) Estimation of tropical rain forest aboveground biomass with small-footprint lidar and hyperspectral sensors. *Remote Sens Environ* 115(11):2931–2942.
37. Lefsky MA, Cohen WB, Parker GG, Harding DJ (2002) Lidar remote sensing for ecosystem studies lidar. *Bioscience* 52(1):19–30.
38. Shugart HH (1984) *A Theory of Forest Dynamics: The Ecological Implications of Forest Succession Models* (Springer, New York).
39. Denslow JS (1987) Tropical rainforest gaps and tree species diversity. *Annu Rev Ecol Syst* 18:431–451.
40. Chambers JQ, et al. (2013) The steady-state mosaic of disturbance and succession across an old-growth Central Amazon forest landscape. *Proc Natl Acad Sci USA* 110(10):3949–3954.
41. Spracklen DV, Righelato R (2014) Tropical montane forests are a larger than expected global carbon store. *Biogeosciences* 11:2741–2754.
42. Phillips OL, Gentry AH (1994) Increasing turnover through time in tropical forests. *Science* 263(5149):954–958.
43. Girardin CAJ, et al. (2010) Net primary productivity allocation and cycling of carbon along a tropical forest elevational transect in the Peruvian Andes. *Glob Change Biol* 16(12):3176–3192.
44. ter Steege H, et al. (2000) An analysis of the floristic composition and diversity of Amazonian forests including those of the Guiana Shield. *J Trop Ecol* 16:801–828.
45. REDD Offset Working Group (2012) *California, Acre and Chiapas: Partnering to Reduce Emissions from Tropical Deforestation*, ed Johnson E (Green Technology Leadership Group, Sacramento, CA).
46. Grassi G, Monni S, Federici S, Achard F (2008) Applying the conservativeness principle to REDD to deal with the uncertainties of the estimates. *Environ Res Lett* 3(3):035005.
47. Grassi G, Federici S, Achard F (2013) Implementing conservativeness in REDD+ is realistic and useful to address the most uncertain estimates. *Clim Change* 119(2):269–275.
48. Plugue D, Baldauf T, Koehl M (2013) The global climate change mitigation strategy REDD: Monitoring costs and uncertainties jeopardize economic benefits. *Clim Change* 119(2):247–259.
49. Köhl M, Baldauf T, Plugue D, Krug J (2009) Reduced emissions from deforestation and forest degradation (REDD): A climate change mitigation strategy on a critical track. *Carbon Balance Manag* 4:10.
50. Asner GP, et al. (2013) High-fidelity national carbon mapping for resource management and REDD+. *Carbon Balance Manag* 8(1):7.
51. Asner GP (2013) Mesoscale exploration and conservation of tropical canopies in a changing climate. *Treetops at Risk: Challenges of Global Canopy Ecology and Conservation*, eds Lowman M, et al. (Springer, New York), pp 177–193.
52. Heffernan JB, et al. (2014) Macrosystems ecology: Understanding ecological patterns and processes at continental scales. *Front Ecol Environ* 12(1):5–14.
53. Malhi Y, et al. (2010) Introduction: Elevation gradients in the tropics: Laboratories for ecosystem ecology and global change research. *Glob Change Biol* 16(12):3171–3175.
54. Asner GP, et al. (2013) Forest canopy gap distributions in the southern Peruvian Amazon. *PLoS ONE* 8(4):e60875.
55. Quesada CA, et al. (2012) Basin-wide variations in Amazon forest structure and function are mediated by both soils and climate. *Biogeosciences* 9:2203–2246.
56. Asner GP, et al. (2012) Carnegie Airborne Observatory-2: Increasing science data dimensionality via high-fidelity multi-sensor fusion. *Remote Sens Environ* 124:454–465.
57. Brokaw N (1982) The definition of treefall gap and its effect on measures of forest dynamics. *Biotropica* 14(2):158–160.
58. Asner GP, et al. (2008) Invasive plants transform the three-dimensional structure of rain forests. *Proc Natl Acad Sci USA* 105(11):4519–4523.
59. Lefsky MA, et al. (1999) Lidar remote sensing of the canopy structure and biophysical properties of Douglas-fir western hemlock forests. *Remote Sens Environ* 70:339–361.
60. Asner GP, et al. (2014) Landscape-scale changes in forest structure and functional traits along an Andes-to-Amazon elevation gradient. *Biogeosciences* 11:843–856.
61. White EP, Enquist BJ, Green JL (2008) On estimating the exponent of power-law frequency distributions. *Ecology* 89(4):905–912.
62. Clauset A, Shalizi CR, Newman MEJ (2009) Power-law distributions in empirical data. *SIAM Rev* 51:661–703.
63. Martin AR, Thomas SC (2011) A reassessment of carbon content in tropical trees. *PLoS ONE* 6(8):e23533.
64. Wang J-F, Stein A, Gao B-B, Ge Y (2012) A review of spatial sampling. *Spat Stat* 2:1–14.
65. Grytnes JA, Vetaas OR (2002) Species richness and altitude: a comparison between null models and interpolated plant species richness along the Himalayan altitudinal gradient, Nepal. *Am Nat* 159(3):294–304.
66. Huasco WH, et al. (2014) Seasonal production, allocation and cycling of carbon in two mid-elevation tropical montane forest plots in the Peruvian Andes. *Plant Ecol Divers* 7(1–2):125–142.
67. R Development Core Team (2012) R: A Language and Environment for Statistical Computing. Available at [www.R-project.org/](http://www.R-project.org/). Accessed July 10, 2014.

# Supporting Information

Marvin et al. 10.1073/pnas.1412999111

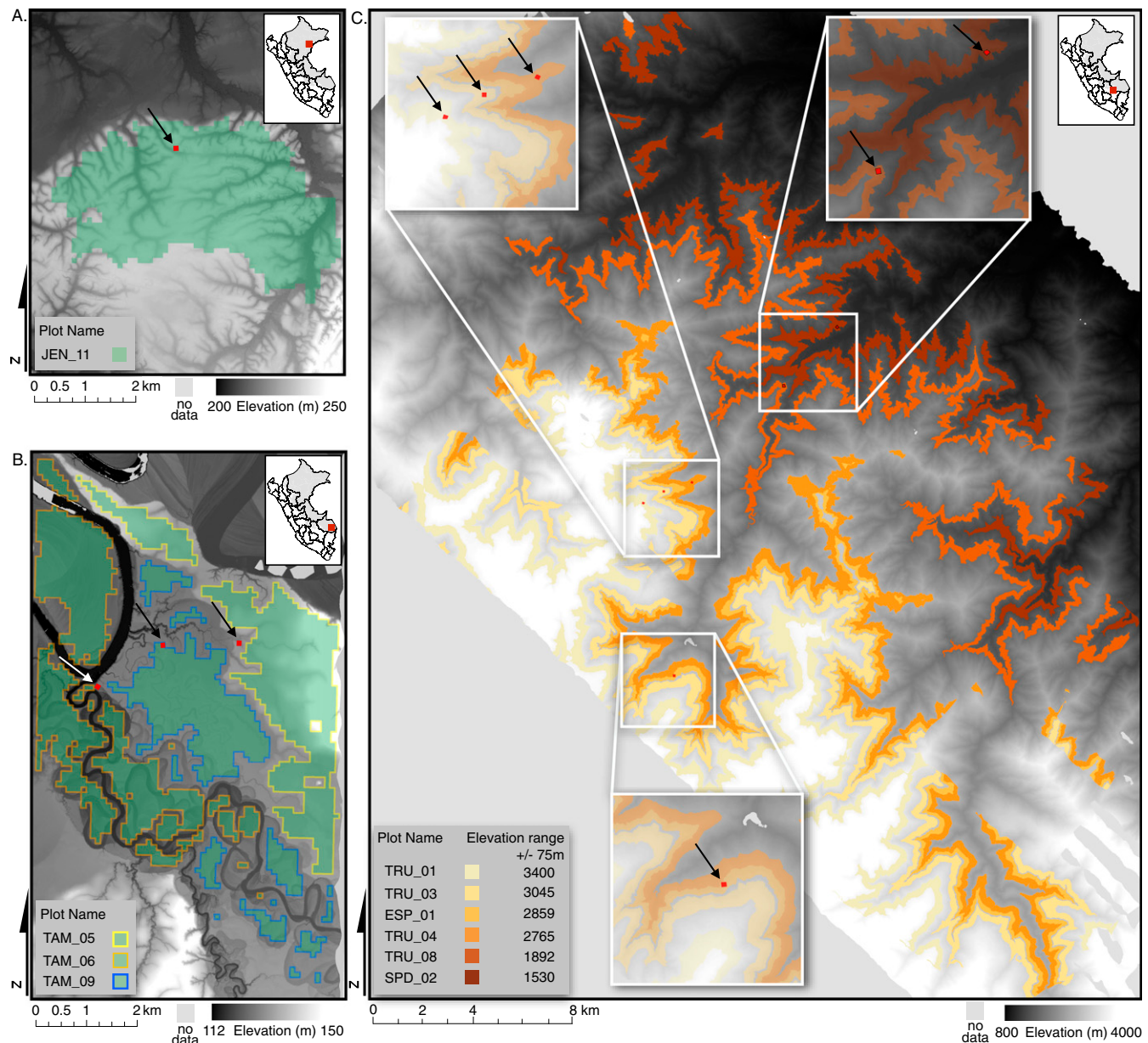


**Fig. S1.** Digital elevation model (DEM) showing the three study regions: (A) Jenaro Herrera, (B) Tambopata, and (C) Kosñipata in Peru. Descriptive information for each landscape is provided in Table 1. Lowland landscapes are shaded in green and differentiated by color outline in B. Montane landscapes are colored by elevation, with zoom insets for detail using the same scaling as in A and B. The location of the 1-ha field inventory plots is shown in red with black arrows for easier identification. Discontinuities in the montane host landscapes are due to gaps in the LiDAR coverage, whereas discontinuities in the lowland host landscapes result from the narrow elevation ranges used to delineate each forest substrate and the removal of grid cells near water features.

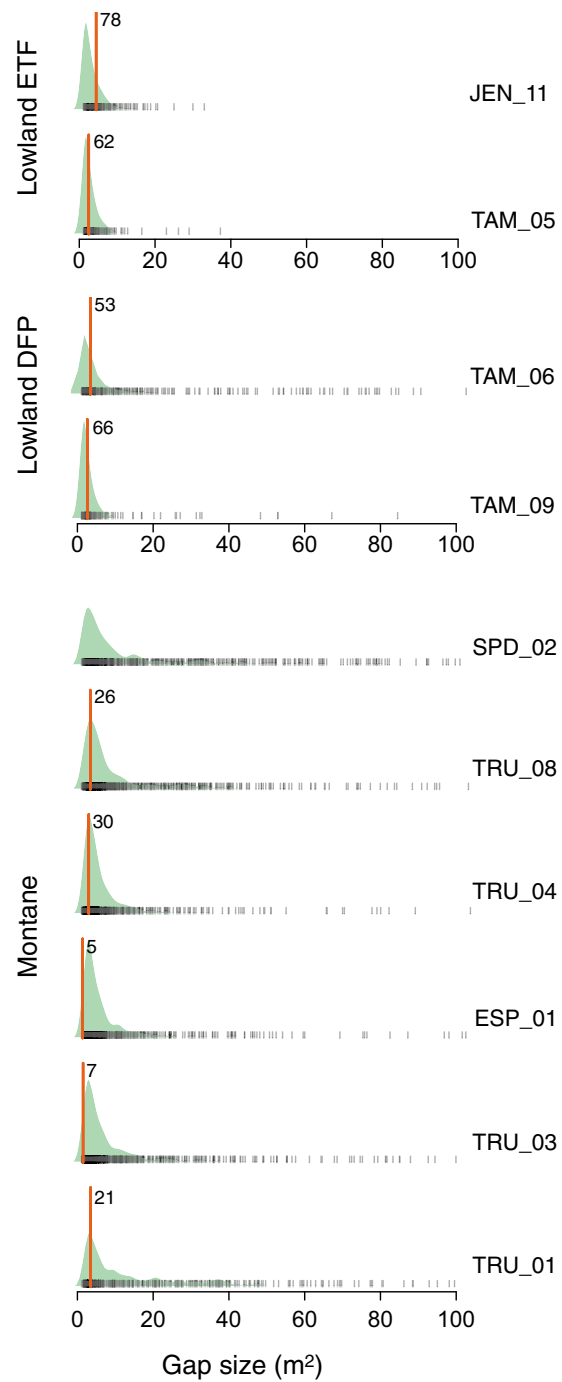


**Fig. S2.** Probability density distributions of gap size (square meters) across landscape grid networks (green), with individual grid cells plotted as small black vertical lines. Red lines are the mean values from the field plots, with adjacent numbers indicating percentile rank within the landscape grid network (determined from the empirical cumulative distribution function). Montane plots are ordered by increasing elevation. Note that the absence of gaps in SPD\_02 means no field-plot gap size can be calculated.

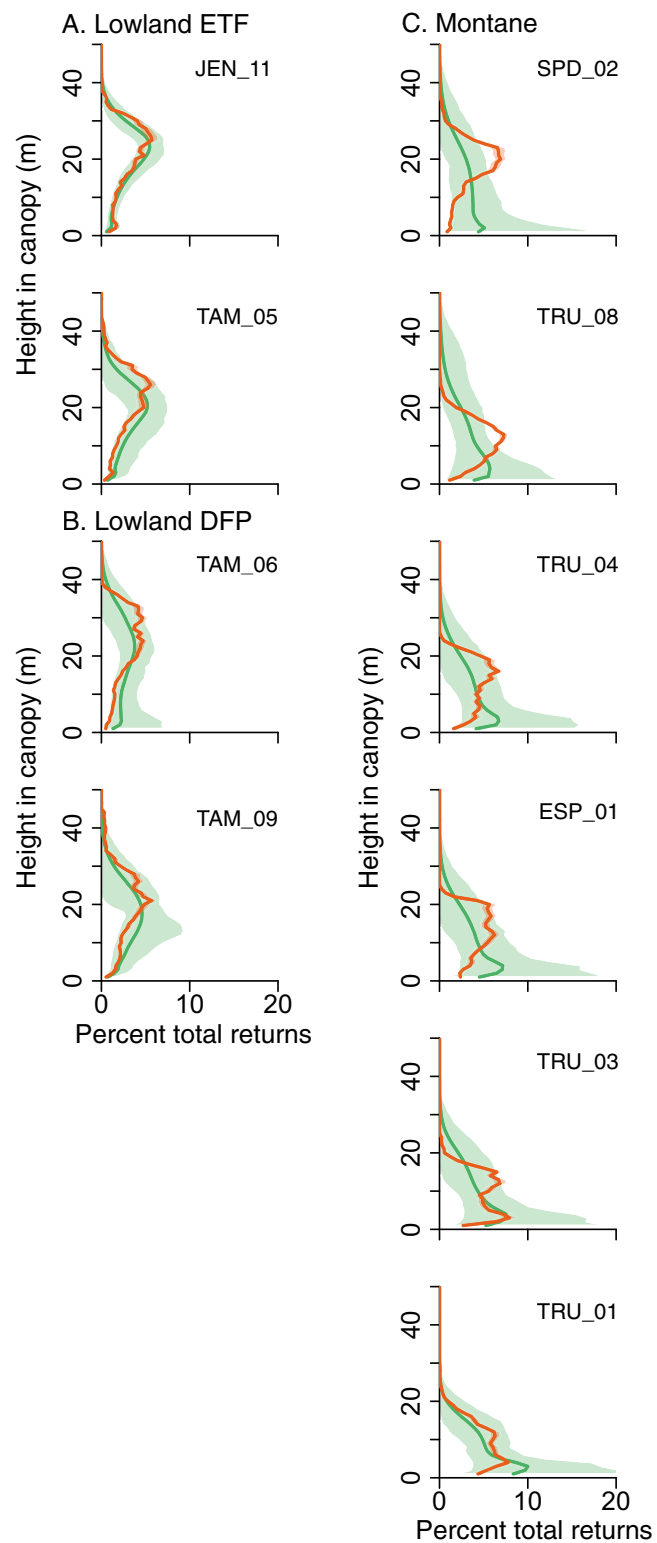


**Fig. S3.** Vertical canopy profiles of the grid networks (green) and the associated field plots (red) for (A) lowland ETF, (B) lowland DFP, and (C) montane landscapes. Solid lines indicate the mean profile and shading is the 95% confidence interval. For the field plots, 95% confidence intervals were obtained from 1,000 bootstrap samples.

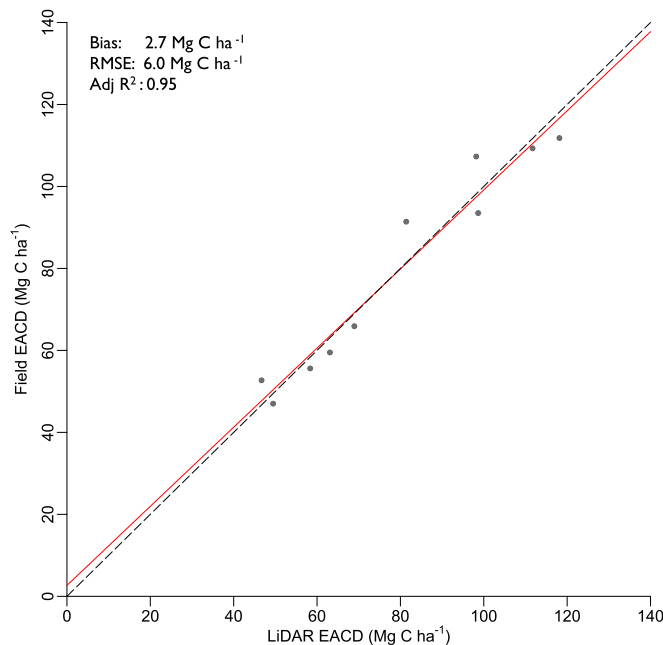


**Fig. S4.** Performance of LiDAR estimated aboveground carbon density (EACD) in predicting field-estimated aboveground carbon density for Andean and Amazonian field plots. The solid red line is the linear regression model fit and the black dashed line is the 1:1 line provided for reference. Bias reflects the mean errors or lack of fit between predicted and observed. RMSE, root mean squared error.

**Table S1. CV of forest structural variables for the host landscape grid network**

Plot	Substrate	Mean TCH, m	P:H	Canopy gap $\lambda$	CV, %	
					Canopy gap density, gaps per hectare	Canopy gap size, m <sup>2</sup>
<b>Lowland</b>						
JEN_11	ETF	6.3	11.5	19.9	99.8	94.8
TAM_06	DFP	15.6	45.3	20.8	105.6	307.5
TAM_09	DFP	17.8	21.4	20.2	97.0	290.3
TAM_05	ETF	12.2	16.9	20.0	95.6	100.1
Average		13.0	23.8	20.2	99.5	198.2
<b>Montane</b>						
SPD_02	Montane	25.2	80.4	16.4	76.4	154.8
TRU_08	Montane	34.8	84.3	14.8	65.6	164.1
TRU_04	Montane	28.0	83.3	15.8	80.9	146.8
ESP_01	Montane	28.6	81.3	16.4	86.0	150.4
TRU_03	Montane	30.2	80.1	17.3	77.8	189.9
TRU_01	Montane	23.8	89.2	12.2	62.3	151.6
Average		28.4	83.1	15.5	74.8	159.6

Higher values indicate more spatial heterogeneity and sampling error. Canopy gap-related variables are derived from gaps at vegetation height  $\leq 2$  m.  $\lambda$ , size-frequency distribution scaling coefficient; P:H ratio, ratio of forest canopy architecture; TCH, top-of-canopy height.

**Table S2. Mean values of structural variables for each field plot and associated host landscape grid network**

Plot	Forest	Max TCH, m				No. of layers			Upper canopy gap $\lambda$			Upper canopy gap density, gaps per hectare			Upper canopy gap size, m <sup>2</sup>		
		Grid network		% $\Delta$ , %	Plot	Grid network		% $\Delta$ , %	Grid network		% $\Delta$ , %	Grid network		% $\Delta$ , %	Grid network		% $\Delta$ , %
		Plot	Plot	% $\Delta$ , %	Plot	Plot	Plot	% $\Delta$ , %	Plot	Plot	% $\Delta$ , %	Plot	Plot	% $\Delta$ , %	Plot	Plot	% $\Delta$ , %
<b>Lowland</b>																	
JEN_11	ETF	31.9	32.8	-2.8	7.0	6.1	14.7	1.63	1.69	-3.8	74.0	76.2	-2.9	28.1	29.8	-5.9	
TAM_06	DFP	35.0	35.3	-1.0	5.0	8.3	-40.0	1.77	1.85	-4.3	107.0	76.5	39.9	13.7	38.9	-64.7	
TAM_09	DFP	33.6	29.2	15.1	8.0	5.8	38.9	1.97	1.84	6.9	71.0	60.1	18.1	40.7	72.5	-43.9	
TAM_05	ETF	34.3	30.9	11.0	8.0	6.6	20.9	1.91	1.76	8.4	80.0	58.9	35.8	25.7	59.2	-56.6	
Average bias				7.5			28.6			5.9			24.1			42.8	
<b>Montane</b>																	
SPD_02	Montane	28.5	28.8	-1.0	7.0	6.5	7.9	NA	NA	NA	NA	NA	NA	NA	NA	NA	NA
TRU_08	Montane	20.0	25.8	-22.6	2.0	5.6	-64.0	NA	NA	NA	NA	NA	NA	NA	NA	NA	NA
TRU_04	Montane	21.5	23.4	-8.3	7.0	4.7	50.0	NA	NA	NA	NA	NA	NA	NA	NA	NA	NA
ESP_01	Montane	20.7	22.4	-7.5	5.0	4.4	14.4	NA	NA	NA	NA	NA	NA	NA	NA	NA	NA
TRU_03	Montane	18.2	20.9	-13.0	4.0	3.8	5.0	NA	NA	NA	NA	NA	NA	NA	NA	NA	NA
TRU_01	Montane	18.2	17.2	6.0	3.0	2.8	7.3	NA	NA	NA	NA	NA	NA	NA	NA	NA	NA
Average bias				9.7			24.8			NA			NA			NA	

% $\Delta$  is the difference between the plot and grid network estimates as a percentage of the grid network. Average bias is the average absolute percent bias. Gap related variables are derived from gaps at vegetation height  $\leq 20$  m (upper canopy). Upper canopy gap variables were not calculated for the montane landscapes.  $\lambda$ , size-frequency distribution scaling coefficient; NA, not applicable; TCH, top-of-canopy height.

**Table S3. CV of forest structural variables for the grid network**

Plot	Forest	CV, %			Upper canopy gap density, gaps per hectare	Upper canopy gap size, m <sup>2</sup>
		Maximum TCH, m	Layers	Gap $\lambda$		
<b>Lowland</b>						
JEN_11	ETF	6.1	28.2	5.0	22.4	52.6
TAM_06	DFP	12.9	27.1	9.4	34.8	280.9
TAM_09	DFP	18.6	41.9	14.0	60.0	337.6
TAM_05	ETF	13.1	32.6	11.5	42.0	421.7
Average		12.7	32.5	10.0	39.8	273.2
<b>Montane</b>						
SPD_02	Montane	21.2	41.0	NA	NA	NA
TRU_08	Montane	25.9	48.9	NA	NA	NA
TRU_04	Montane	24.1	51.7	NA	NA	NA
ESP_01	Montane	25.9	54.0	NA	NA	NA
TRU_03	Montane	26.2	55.3	NA	NA	NA
TRU_01	Montane	17.4	44.3	NA	NA	NA
Average		23.5	49.2	NA	NA	NA

Higher values indicate more spatial heterogeneity and sampling error. Gap related variables are derived from gaps at vegetation height  $\leq 20$  m (upper canopy). Upper canopy gap variables were not calculated for the montane landscapes.  $\lambda$ , size-frequency distribution scaling coefficient; NA, not applicable; TCH, top-of-canopy height.

**Table S4.** Mean values of all structural and biomass variables for each grid network and associated ungridded host landscape

Plot	Forest	Mean TCH, m			P:H ratio			Canopy gap $\lambda$			Canopy gap size, m <sup>2</sup>			Layers			Upper canopy gap $\lambda$			Upper canopy gap size, m <sup>2</sup>			LiDAR EACD, Mg C·ha <sup>-1</sup>				
		Host	% $\Delta_{\lambda}$	Grid landscape %	Host	% $\Delta_{\lambda}$	Grid landscape %	Host	% $\Delta_{\lambda}$	Grid landscape %	Host	% $\Delta_{\lambda}$	Grid landscape %	Host	% $\Delta_{\lambda}$	Grid landscape %	Host	% $\Delta_{\lambda}$	Grid landscape %	Host	% $\Delta_{\lambda}$	Grid landscape %	Host	% $\Delta_{\lambda}$	Grid landscape %		
Lowland																											
JEN_11	ETF	22.6	23.2	-2.7	0.6	0.81	-26.2	1.94	1.88	3.3	3.7	3.8	-2.2	6.1	7.3	-15.9	1.69	1.74	-3.1	29.8	31.7	-5.8	115.4	120.0	-3.8		
TAM_06	DFP	22.0	22.9	-3.7	0.47	0.77	-38.8	1.86	1.78	4.4	19.2	20	-4	8.3	7.2	15.9	1.85	1.92	-4	38.9	40.5	-4.1	89.6	93.7	-4.5		
TAM_09	DFP	18.8	19.4	-3.2	0.52	0.78	-32.6	2.03	1.95	4	6.1	6.2	-1.8	5.8	6.5	-12	1.84	2.01	-8.5	72.5	75.5	-3.9	69.8	72.2	-3.4		
TAM_05	ETF	20.2	20.9	-3.1	0.55	0.8	-30.9	2.04	1.94	5	3.4	3.5	-1.9	6.6	6.8	-2.2	1.76	1.86	-5.5	59.2	62.5	-5.3	77.7	81.1	-4.1		
Average bias																											
Montane																											
SPD_02	Montane	16.0	16.9	-5.3	0.24	0.64	-62.9	1.77	1.69	4.6	20.5	21.1	-3.0	6.5	5.9	9.8	NA	NA	NA	NA	NA	NA	NA	NA	NA	NA	
TRU_08	Montane	13.8	14.7	-6.1	0.19	0.59	-67	1.79	1.71	4.3	13.8	14	-1.8	5.6	5.5	1	NA	NA	NA	NA	NA	NA	NA	NA	NA	NA	
TRU_04	Montane	12.6	13.4	-6.1	0.21	0.6	-65	1.88	1.77	5.8	8.7	8.8	-1.5	4.7	5.1	-9.1	NA	NA	NA	NA	NA	NA	NA	NA	NA	NA	
ESP_01	Montane	12.0	12.9	-6.6	0.21	0.6	-65.5	1.88	1.77	6.6	11.1	11.2	-1.3	4.4	5	-12.4	NA	NA	NA	NA	NA	NA	NA	NA	NA	NA	
TRU_03	Montane	11.4	12.2	-6.9	0.19	0.6	-68.1	1.87	1.76	6.4	13.4	13.7	-1.8	3.8	4.8	-19.8	NA	NA	NA	NA	NA	NA	NA	NA	NA	NA	
TRU_01	Montane	9.0	9.7	-6.8	0.15	0.59	-74.5	1.81	1.81	0.3	17.9	18.4	-2.3	2.8	4	-29.6	NA	NA	NA	NA	NA	NA	NA	NA	NA	NA	
Average bias																											

$\%_{\Delta}$  is the difference between the grid network and ungridded host landscape as a percentage of the ungridded host landscape. Average bias is the average absolute percent bias. Upper canopy gap (vegetation height  $\leq 20$  m) variables were not calculated for the montane landscapes. EACD, estimated aboveground carbon density;  $\lambda$ , size-frequency distribution scaling coefficient; NA, not applicable; P:H ratio, ratio of forest canopy architecture; TCH, top-of-canopy height.

**Table S5. Number of field plots needed per landscape to achieve different levels of accuracy in estimating the landscape grid mean EACD at four different probabilities**

Plot	Substrate	95% accuracy				90% accuracy				80% accuracy			
		0.9	0.8	0.7	0.6	0.9	0.8	0.7	0.6	0.9	0.8	0.7	0.6
<b>Lowland</b>													
JEN_11	ETF	38	23	15	10	10	6	4	3	3	2	1	1
TAM_06	DFP	>100	>100	90	61	58	37	24	16	15	10	6	4
TAM_09	DFP	>100	>100	>100	75	71	44	29	20	20	12	8	5
TAM_05	ETF	>100	81	56	38	37	22	15	10	9	6	4	2
Average		>85	>76	>65	46	44	27	18	12	12	8	5	3
<b>Montane</b>													
SPD_02	Montane	>100	>100	>100	75	75	46	31	21	20	12	8	5
TRU_08	Montane	>100	>100	>100	>100	>100	88	57	41	37	23	16	10
TRU_04	Montane	>100	>100	>100	>100	95	60	41	27	27	16	10	7
ESP_01	Montane	>100	>100	>100	>100	>100	61	41	28	27	17	11	7
TRU_03	Montane	>100	>100	96	96	98	75	47	33	30	19	12	8
TRU_01	Montane	>100	>100	>100	75	70	46	31	21	20	12	8	6
Average		>100	>100	>100	>91	>85	63	41	29	27	17	11	7

A maximum sample size of 100 field plots was assessed. EACD, estimated aboveground carbon density.

**Table S6. Locations of the field plots published by RAINFOR and ABERG, along with information on host landscape assessment**

Landscape	Plot	Latitude	Longitude	Elevation, m	Landscape size, ha	Forest substrate	MAT, °C	MAP, mm	Soils
<b>Lowland</b>									
Jenaro Herrera	JEN_11	-4.8781	-73.6295	131.2	1,252	ETF	26.6	2,700	Ultisol
Tambopata	TAM_06	-12.8385	-69.2960	214.8	874	DFP	24.0	2,600	Inceptisol
Tambopata	TAM_09	-12.8309	-69.2843	219.2	616	DFP	24.0	2,600	Inceptisol
Tambopata	TAM_05	-12.8303	-69.2705	223.3	750	ETF	24.0	2,600	Ultisol
<b>Montane</b>									
San Pedro	SPD_02	-13.0491	-71.5365	1,712.9	1,017	Montane	18.5	4,628	Inceptisol
Mirador	TRU_08	-13.0702	-71.5559	1,831.5	1,014	Montane	18.5	4,341	Entisol
Trocha Union	TRU_04	-13.1055	-71.5893	2,719.1	913	Montane	13.0	2,678	Inceptisol
Esperanza	ESP_01	-13.1751	-71.5948	2,868.3	863	Montane	12.5	1,705	Inceptisol
Trocha Union	TRU_03	-13.1097	-71.5995	2,989.5	1,011	Montane	13.0	2,678	Inceptisol
Trocha Union	TRU_01	-13.1136	-71.6069	3,379.3	526	Montane	8.0	2,448	Inceptisol

MAP, mean annual precipitation; MAT, mean annual temperature. All montane landscapes are in the Kosñipata Valley.